APPLIED SCIENCES AND ENGINEERING

Optogenetic-induced muscle loading leads to mechanical adaptation of the Achilles tendon enthesis in mice

Elahe Ganji[1,2,3]†, Syeda N. Lamia[1,4]†, Matthew Stepanovich[1], Noelle Whyte[1], Robert W. Goulet[1], Adam C. Abraham[1], Megan L. Killian[1,3]*

Copyright © 2023 The Authors, some rights reserved; exclusive licensee American Association for the Advancement of Science. No claim to original U.S. Government Works. Distributed under a Creative Commons Attribution NonCommercial License 4.0 (CC BY-NC).

Skeletal shape depends on the transmission of contractile muscle forces from tendon to bone across the enthesis. Loss of muscle loading impairs enthesis development, yet little is known if and how the postnatal enthesis adapts to increased loading. Here, we studied adaptations in enthesis structure and function in response to increased loading, using optogenetically induced muscle contraction in young (i.e., growth) and adult (i.e., mature) mice. Daily bouts of unilateral optogenetic loading in young mice led to radial calcaneal expansion and warping. This also led to a weaker enthesis with increased collagen damage in young tendon and enthisis, with little change in adult mice. We then used RNA sequencing to identify the pathways associated with increased mechanical loading during growth. In tendon, we found enrichment of glycolysis, focal adhesion, and cell-matrix interactions. In bone, we found enrichment of inflammation and cell cycle. Together, we demonstrate the utility of optogenetic-induced muscle contraction to elicit in vivo adaptation of the enthesis.

Downloaded from https://www.science.org on July 08, 2024

INTRODUCTION

The enthesis is a tissue interface that adapts to applied muscle loads during postnatal growth by forming a graded fibrocartilage transition between tendon and bone (*1*–*4*). The mature enthesis is a network of mineralized and unmineralized collagen fibers that is tougher than either tendon or bone (*5*). As the result of this structural toughening, acute and high-energy–induced injuries typically involve failure of tendon (e.g., Achilles tendon ruptures) or bone (e.g., calcaneal avulsion fractures) and not the enthesis (*6*). However, with chronic and repetitive loading, the enthesis is susceptible to localized damage and overuse-related injuries. In fact, up to 25% of all chronic tendon and ligament disorders involve the enthesis (*7*–*10*). Overuse is considered the underlying cause of most entheseal disorders (e.g., Achilles insertional tendinopathy and Sever disease) that are disproportionately observed in young athletes (*7*, *11*, *12*). For example, Sever disease, classified as pain adjacent to the Achilles enthesis, is considered an inflammatory condition of the calcaneal apophysis caused by high levels of physical activities in children (*13*). However, there does exist uncertainty related to this diagnosis due to a lack of clear evidence regarding its pathophysiology.

Yet, loading is essential for functional development and growth of the tendon-bone enthesis (*9*, *14*–*16*). During embryonic development, the tendon extends from the cartilage anlagen to guide load transfer from skeletal muscle, which induces the mechano-adaptive growth of the enthesis (*17*). During postnatal development, the enthesis matures into a graded fibrocartilage interface from the fibrous tendon to the mineralized bone (*9*, *14*). The structural adaptation of the enthesis occurs in response to a combination of tensile, shear, and compressive loads (*4*, *9*, *18*). While several elegant studies have established the requirement of muscle contraction during musculoskeletal growth, these studies have primarily focused on the absence or reduction of muscle loading rather than increased muscle contraction (*17*, *19*, *20*). Yet, increased activity during periods of rapid growth, such as in children and during adolescence, is associated with micromotion at the enthesis and apophysis and results in pain and presentation of disorders such as Sever disease (*7*, *8*). In adults, repeated tendon loading during activities such as running-associated overuse can lead to abnormalities such as bony spur formation at the distal tendon that leave individuals with pain and dysfunction (*2*, *9*). Despite the potential age-associated differences in adaptation of the enthesis to repeated loading, the mechanisms contributing to enthesis adaptation of the immature and mature skeleton remain poorly understood and challenging to study (*21*).

In mouse and rat studies of the skeletal adaptation to mechanical loading, cyclic, subfailure compressive loading has commonly been used to induce anabolic bone formation in both the ulna and tibia (*22*–*26*). Similarly, subfailure cyclic tensile loading of the patellar tendon has been used to model tendon fatigue and damage in mice and rats (*27*, *28*). Unfortunately, the latter approach does not load tendon enthesis via muscle contraction but instead via direct, open, and external mechanical actuation. More commonly used and physiologically relevant models of tendon loading, such as forced treadmill running (uphill or downhill), are effective for inducing structural changes to the mature enthesis in response to increased loading but also have their drawbacks (*29*–*32*). For example, treadmill running studies in mice and rats, such as most bone anabolic loading studies, typically initiate forced running at 7 to 8 weeks of age (*33*), which limits our ability to study tendon and enthesis adaptation during maturation. In addition, these approaches are highly variable, as even inbred mouse strains have high variations in distances run and tolerance for forced treadmill running

[1]Department of Orthopaedic Surgery, Michigan Medicine, University of Michigan, 109 Zina Pitcher Pl., Ann Arbor, MI 48109, USA. [2]Beckman Institute for Advanced Science and Technology, University of Illinois at Urbana-Champaign, 405 North Mathews Ave., Urbana, IL 61801, USA. [3]Department of Biomedical Engineering, University of Delaware, 540 S. College Ave., Newark, DE 19713, USA. [4]Department of Mechanical Engineering, University of Michigan, 2350 Hayward St., Ann Arbor, MI 48109, USA.
*Corresponding author. Email: mlkillia@med.umich.edu
†These authors contributed equally to this work.

(*34*). Forced treadmill running can also confound the results by inducing anxiety, lead to systemic inflammation (*35*) and effect organismal metabolic conditioning induced by cardiovascular load and training (*36*). To counter the systemic effects and reduce loading dose variability, electrical nerve stimulation has also been used to induce repeated muscle stimulation in mice and rats for tendon loading (*37*, *38*). However, this approach is also challenging, as most studies are in adult animals and these approaches require subdermal needle electrode placement, which may increase the risk of injury and infection with repeated electrode placement in the growing muscle and tendon. Thus, understanding how loading affects structural changes to the tendon enthesis during growth has been challenging in vivo because of a lack of physiologically relevant loading models.

To address these challenges, we turned to the use of optogenetics as a noninvasive tool for direct and precise induction of muscle contraction for in vivo tendon loading in growing mice. Optogenetics is a tool commonly used in neuroscience that facilitates controlled activation of activatable cells such as neurons and muscle cells, with high spatial and temporal specificity (*39*). Channelrhodopsin-2 (ChR2) is a light-sensitive microbial opsin that, when present on the cell membrane, acts as a nonspecific light-activated cation channel that induces membrane depolarization (*40*, *41*). Optogenetic stimulation improves the spatial specificity of electrical stimulation by targeting cell subpopulations based on morphological markers and molecular footprint (*42*). We and others have previously shown that optogenetic-mediated activation of skeletal muscle allows for precise and controlled contraction of specific muscle groups (*43*–*45*) and, therefore, their associated tendons and entheses. In this study, we used pulsatile transcutaneous exposure of *ChR2*-expressing skeletal muscle cells to collimated blue light-emitting diode (LED) light (455 nm) to induce isometric activation of triceps surae muscles. We examined how sustained daily bouts of optogenetic activation can differentially elicit structural, functional, and molecular changes in the young and adult Achilles enthesis of mice. We then defined transcriptional changes in the young tendon and bone following repeated loading.

RESULTS

Optogenetic activation is a repeatable and safe approach for daily tendon loading

To investigate the effects of increased loading on the postnatal Achilles enthesis, we generated a transgenic mouse line to express *ChR2* in skeletal muscle [doxycycline-treated Ai32-floxed, ACTA1-rtTA;tetO-Cre mice (*44*)] and unilaterally loaded their Achilles tendon using optogenetic stimulation of the triceps surae muscle (Fig. 1). Daily bouts of loading were delivered under isoflurane anesthesia at either 5- or 20-min bouts for 5 days a week, up to 3 weeks (19 days) in duration, in mice starting at either 4 weeks of age (young group; this time point coincides with enthesis growth) or at 6 to 8 months of age (adult group, 20-min bouts only; mature enthesis) (Fig. 1). In young mice, the steady state–generated torque at the end of the 20-min loading bout was ~30% of the initial peak torque for the first week of daily optogenetic muscle loading. We found that daily loading in young mice did not negatively affect the animal weight gain; however, some weight loss was observed in adult mice (Fig. 2A). Isometric ankle joint torque did not significantly vary over the course of the experiment for the young group but did increase with daily 20-min loading bouts in the adult group from week 1 to week 2 of loading (Fig. 2B). A subset of mice were used to measure ankle torque for the first five consecutive days and throughout the duration of loading. Peak torque (~3 N-mm), generated by the hindlimb muscles in young mice, was measured in the first one to two cycles of loading (cycle = 70-ms light on, 30-ms light off; every 5 s), and steady-state torque (~1 N-mm) was generated around 500 to 750 cycles (~100 to 125 cycles) (Fig. 2C). To test the response to optogenetic stimulation in adult mice, we isolated the extensor digitorum longus (EDL) muscle from an adult (3-month-old) mouse treated with doxycycline during gestation and up to weaning (21 days of age) and measured twitch forces in vitro in response to blue light exposure. We were able to elicit strong and duration-dependent force generation, which indicates sufficient ActaCre-*ChR2* recombination (Fig. 2D).

Daily tendon loading leads to bony changes and impaired mechanical properties of the young but not adult Achilles enthesis

Daily loading of the tendon and enthesis for 3 weeks (19 days) led to apophyseal shape changes in the young calcanei (Fig. 3A). Quantitative differences in the shape of the young calcaneus in response to optogenetic-induced loading were measured as three major mode shape changes, namely shortening (mode 1: 63.7% shape change; shown in blue in Fig. 3A on deformation maps in posterior view), expansion/breathing mode (mode 2: explaining 13.3% shape change), and warping (mode 3: highlighted in Fig. 3A; shown in red on deformation maps in both lateral and medial views). The adult loaded calcaneus was not significantly different in length compared to control calcaneus, and we did not measure differences in tissue volume (TV) or bone volume (BV) percentage (BV/TV) with loading compared to contralateral controls. However, the young calcaneus was smaller in volume with loading and had increased BV/TV (Fig. 3B). Neither young (Fig. 3B) nor adult exhibited a statistically significant change in length from the calcaneal tuberosity to the peroneal tubercle. With shorter loading bouts (i.e., 5 min loading duration), we did not observe any significant differences in young calcaneal length, TV, or BV/TV compared to contralateral controls (table S1).

All tissues failed at the enthesis (young and adult) or calcaneal growth plate (young), not the tendon mid-substance, during uniaxial testing. In Young mice, the maximum load before failure was significantly reduced following repeated loading compared to the contralateral Achilles tendon and enthesis (Fig. 3C). However, increased strength was observed in the adult tendon/enthesis following 3 weeks of loading compared to the contralateral tendons (Fig. 3C). For the young, but not adult, Achilles tendon/enthesis toughness was significantly reduced after 3 weeks of loading compared to contralateral tendons (Fig. 3C).

Daily tendon loading leads to accumulated collagen damage in young mice

Loading can initiate accumulative damage at the molecular level by inducing fibril breaks and protease-induced remodeling of the extracellular matrix (ECM). As a result of this ECM damage, collagen triple helices can irreversibly unfold (*46*). To evaluate collagen damage in our in vivo model of tendon loading, we used collagen hybridizing peptides (CHPs) conjugated with fluorescent labels to visualize molecular-level damage (*47*, *48*). In tendon, CHPs can

Downloaded from https://www.science.org on July 08, 2024

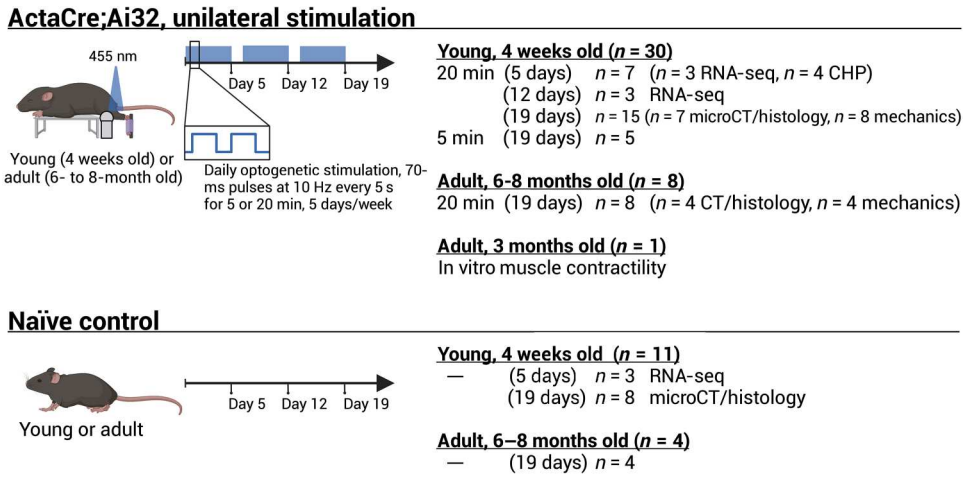

Fig. 1. Study design: Schematic of experimental setup for optogenetic muscle loading (shown here for young mice). Right hindlimbs of young and adult ActaCre;Ai32 mice were exposed to daily bouts of either 5- or 20-min optogenetic-induced muscle contractions of the triceps surae. Mice were used experimentally after various loading bouts, including for RNA sequencing (RNA-seq) (young mice only; after 5 or 12 days of 20-min loading); for collagen damage assays [collagen hybridizing peptide (CHP); young mice only, after 5 days of 20-min loading]; for microcomputed tomography (young and adult mice; 19 days of 20-min loading); and for mechanical testing (young and adult mice; 19 days of 20-min loading). At each designated end point (i.e., experimental days 5, 12, or 19), experimental and naïve age-matched controls were euthanized to collect Achilles tendon and enthesis for histology, micro–computed topography (microCT), and mechanics and Achilles tendon and calcaneus for RNA isolation (RNA-seq). Created with BioRender.com.

specifically detect the nonrecoverable (post-yield) unfolding of collagen fibers (*46*). After five consecutive days of 20-min daily loading bouts, young loaded tendon and enthesis had higher CHP intensity (Fig. 4B) and, therefore, collagen denaturation than contralateral controls ($P = 0.0074$). Collagen type III is correlated with increased remodeling; however, the attachments did not have quantitatively more collagen-type III$^+$ cells or aggrecan within the enthesis compared to controls (Fig. 4, C and E) following 3 weeks (19 days) of loading. Histologically, we also observed thinning of the young fibrocartilage enthesis and smaller, but not fewer, cells with loading (Fig. 4, D and F). We did not observe any major morphological differences between loaded young entheses with 5-min daily loading bouts compared to 20-min bouts (fig. S1).

Daily bouts of optogenetic loading leads to acutely down-regulated gene expression in both tendon and bone

We performed bulk RNA sequencing (RNA-seq) with RNA isolated from Achilles tendons and calcanei of naïve and optogenetically loaded young mice (loaded and contralateral limbs) at 4 hours post-final loading bout to investigate the molecular changes underlying the structural enthesis and bone morphology. We used principal components analyses (PCAs) to evaluate data quality in an unsupervised approach (Fig. 5A). To avoid any compensatory effects of the contralateral limb and because we saw a discrete separation of naïve from loaded (5 and 12 days) tendons in PCA, we used naïve data to measure fold change between optogenetically loaded and cage activity tendons and bones (Fig. 5A). We identified 1193 and 312 genes in tendon and bone, respectively, that were differentially expressed at both 5 and 12 days of loading (Fig. 5, B and C), and both tendon and bone had more differentially expressed genes (DEGs) at 12 days compared to 5 days of daily loading. A full list of DEGs is provided in data S1.

We used the Database for Annotation, Visualization, and Integrated Discovery (DAVID) to further analyze biological processes and Kyoto Encyclopedia of Genes and Genomes (KEGG) pathways. We found that several biological processes were enriched in both tendon and bone, including angiogenesis, ECM organization, cellular response to transforming growth factor–β stimulus, and response to mechanical stimulus (Fig. 6). In addition, in tendon, we found that fibroblast growth factor (FGF) receptor signaling was enriched after 5 days of loading, and canonical glycolysis was enriched after 12 days of loading (Fig. 6A). In bone, we found that integrin-mediated signaling and inflammatory response were enriched after 12 days of loading and collagen fibril organization, and DNA replication initiation was enriched after 12 days of loading (Fig. 6B).

We found that optogenetic loading resulted in down-regulation of numerous genes associated with tendon stem cells, including *Tppp3*, *Tnc*, and *Fbn1*, which were down at both 5 and 12 days (Fig. 7). Of the top 20 down-regulated genes [based on $\log_2$-transformed fold change (log2FC)] in tendon following loading, most were associated with ECM synthesis at one or both time points, including *Matn3*, *Acan*, *Col8a1*, *Thbs1*, *Col9a2*, *Bglap*, *Mmp9*, *Col2a1*, and *Adamts19* (Fig. 7). This was further confirmed using KEGG pathway analysis in DAVID, in which focal adhesion, ECM-receptor interaction, and regulation of actin cytoskeleton were significantly enhanced at both 5- and 12-day time points (Fig. 8A). ECM-receptor interaction was significantly down-regulated with loading in tendon at both 5 and 12 days compared to naïve control tendons (Fig. 8C). In bone, daily bouts of loading resulted in increased expression of *Il1ra2*, *Ccl21c*, *Ccl21a*, *Gpnmb*, and *Ccl19* and other pro-inflammatory markers at one or both time points (Fig. 7). We also found that *Ihh* was one of the top 20 down-regulated genes in bone at both 5 and 12 days with loading (Fig. 7). Activation of the KEGG pathway, focal adhesion, identified bout-dependent changes in gene expression, especially for *Tnc*, *Col1a1*, *Col1a2*, and *Thbs4* in bone (Fig. 8D). Expression of *Tnc*, as well as *Col1a1*, *Col1a2*, and *Col2a1*, were consistent in follow-up experiments using real-time quantitative reverse transcription polymerase

Downloaded from https://www.science.org on July 08, 2024

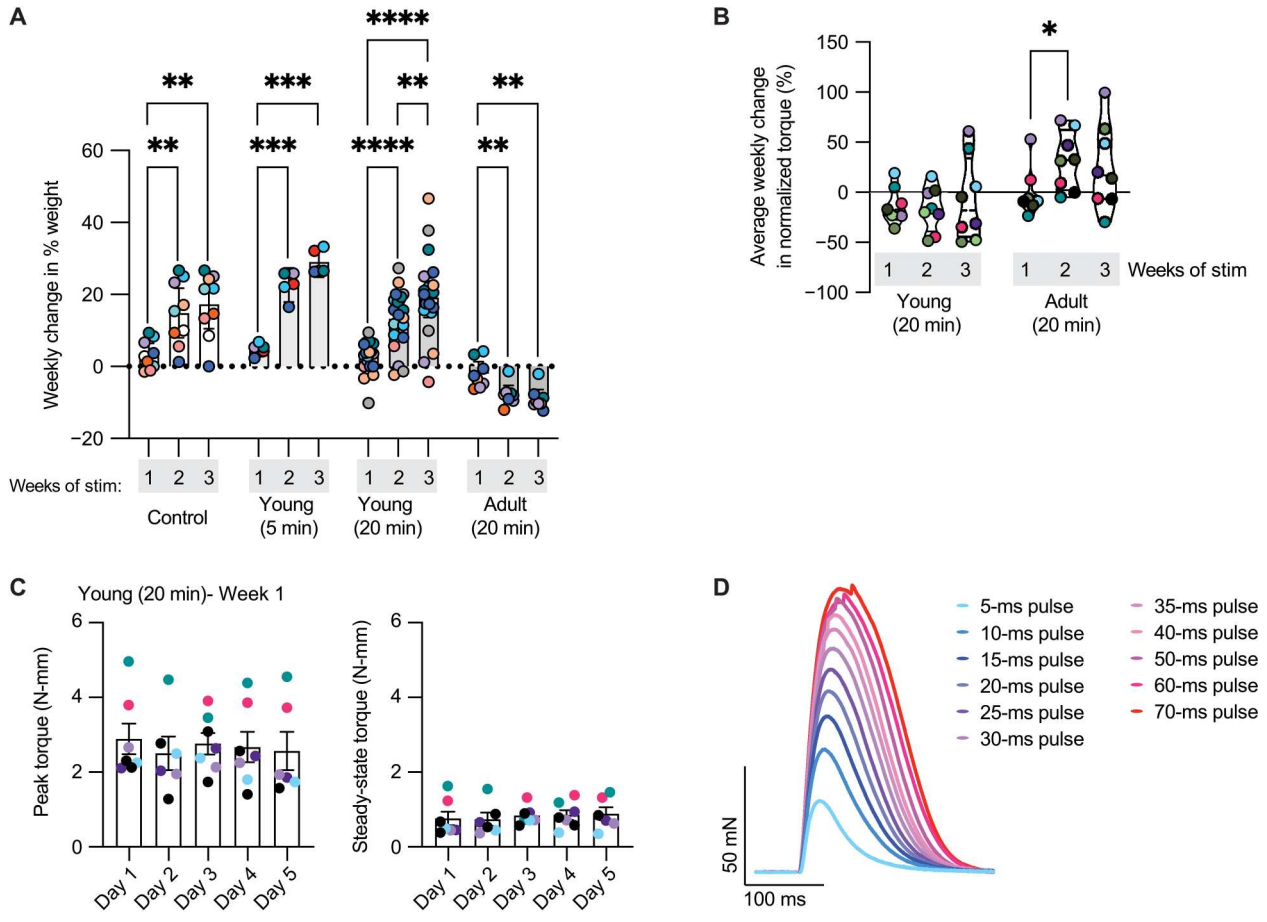

Fig. 2. Optogenetic activation of triceps surae muscle group is not invasive and does not negatively influence animal weight or generated isometric ankle joint torque in young mice. (**A**) Young mice, regardless of exposure to daily bouts of optogenetic muscle stimulation (5- or 20-min duration), gained weight for the duration of the experiment. However, adult mice lost weight (~10%) from onset to end of the experiment. Controls were naïve mice at similar ages as the young group. (**B**) Normalized torque significantly increased in adult but not young mice with daily bouts of 20-min optogenetic muscle stimulation. Each data point denotes the average weekly change in generated ankle torque normalized to the weight of the animal. (**C**) Steady state–generated ankle torque (at the end of the 20-min loading bout), measured during isometric ankle plantarflexion, was ~30% of the peak torque in young mice for the first week of daily optogenetic muscle loading. (**D**) EDL muscle from an adult (3-month-old) ActaCre;Ai32 mouse had a duration-dependent force response to blue light exposure measure contraction when tested in vitro (5 to 70 ms). For (A) and (B), data were compared using two-way analysis of variance (ANOVA) with mixed models (repeated measures between weeks within groups, Sidak correction). Error bars denote means ± 95% confidence interval. *P < 0.05, **P < 0.001, ***P = 0.0004, and ****P < 0.0001.

chain reaction (qRT-PCR) on cDNA from tendon RNA samples used in RNA-seq (fig. S2).

DISCUSSION

In this study, we evaluated the mechanically induced adaptation of both the young and adult enthesis to repeated loading using optogenetic stimulation. Previous studies have explored the effects of repeated loading on the structural and functional adaptation of healthy and repaired tendon and enthesis in adult and aging tissues (*29*, *49*–*52*). Yet, the effect of repeated loading on immature tendon and enthesis was previously unknown. We used optogenetic stimulation of triceps surae muscle to induce ankle joint plantar flexion with comparable generated joint torques to electrically induced nerve stimulation (*44*). We leveraged pulsatile light-induced activation of ChR2 in skeletal muscle cells for repeated tensile loading of the Achilles tendon and enthesis. Optogenetic activation of skeletal muscle was noninvasive and did not cause weight loss or gross macroscopic damage to the tendon or enthesis after 3 weeks. Repeated loading did result in microscopic changes and disruption of the structure and function of the young, but not the adult enthesis. Repeated loading also led to opening of the growth plate, disruption of the enthesis tidemark, and impaired mechanical properties in young mice. This may have been caused by disruption of the continuous transition between the mineralized and unmineralized fibrocartilage of the enthesis that contributes to the tissue's mechanical toughness (*53*) and is the primary determinant of enthesis mechanics and stress transfer between tendon and bone (*54*).

In tendons, aging leads to impaired self-renewal potential (*55*), tissue turnover (*56*), increased prevalence of proteoglycans and mineral (*57*), and degenerative structural adaptations (e.g., reduced cellularity, disruption of collagen fiber orientation, and fibroblastic changes) (*56*, *57*). In mice, reduced tendon stem cell

Downloaded from https://www.science.org on July 08, 2024

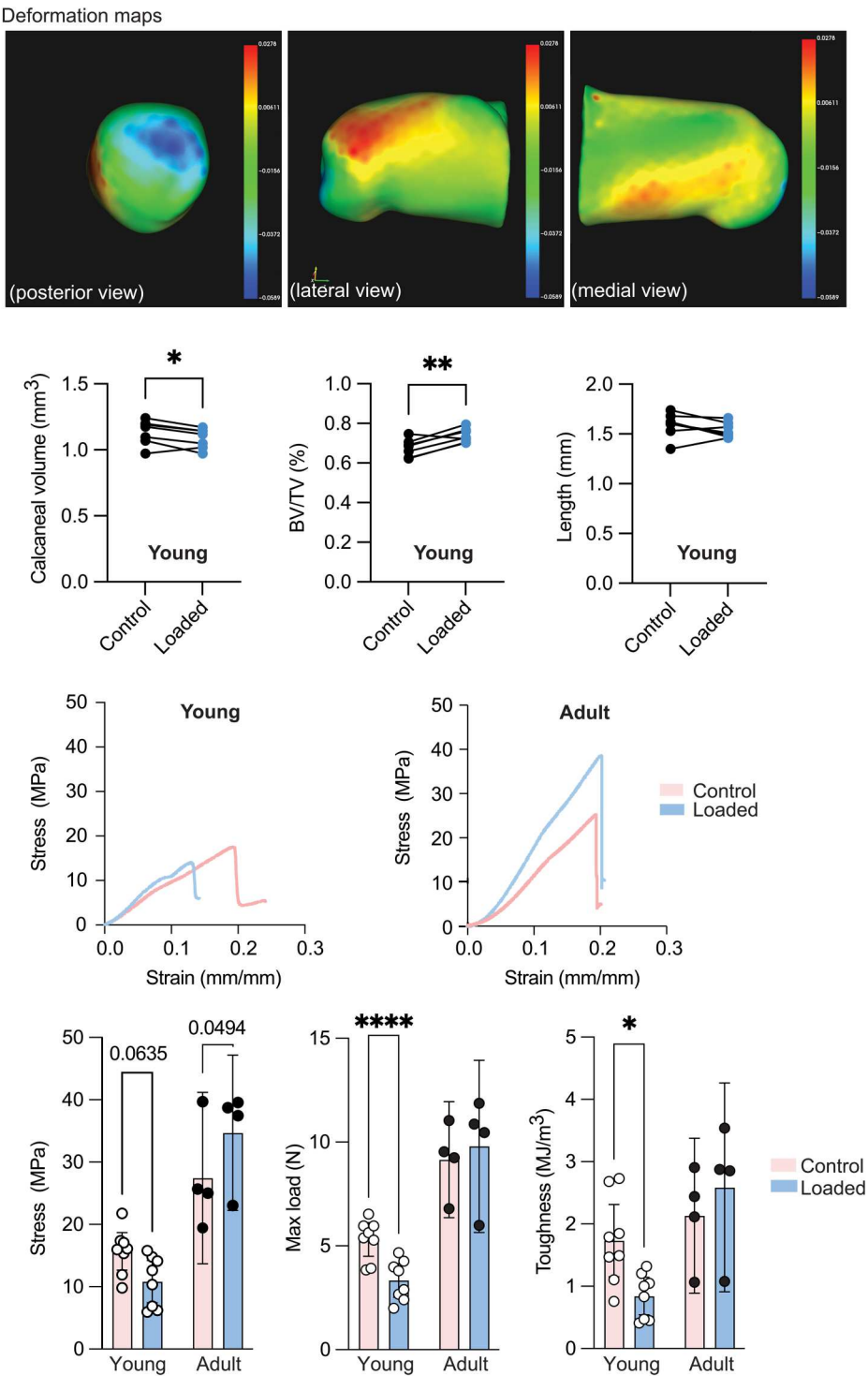

Fig. 3. Repeated daily loading of Young mouse Achilles tendons results in expansion and warping deformation and impaired mechanical toughness at the enthesis. (**A**) Deformation maps of the posterior, lateral, and medial views of loaded (average shape; right calcaneus) compared to control (average shape, left calcaneus, mirrored for overlay/shape representation) showed reduced height of the calcaneal tuberosity with loading (posterior view; shown in blue) and increased bone expansion and warping (lateral and medial views; shown in red). (**B**) Total volume of the calcaneal region of interest was significantly reduced with loading (paired *t* test; $P = 0.0338$), and BV/TV (%) was significantly increased (paired *t* test; $P = 0.0056$) in young loaded compared to young control calcanei. No significant differences in length between young control and loaded calcanei were measured. (**C**) Representative stress-strain curves for young and adult groups showed structural adaptations in the young enthesis and apophysis coincide with significantly reduced tensile strength and toughness in the loaded compared to nonloaded contralateral limbs. Data were compared using two-way ANOVAs with multiple comparisons (contralateral versus loaded; no correction for sphericity; Sidak correction for multiple comparisons). Error bars denote means ± 95% confidence interval. $*P < 0.05$, $**P < 0.01$, $***P < 0.001$, and $****P < 0.0001$.

proliferation has been reported as early as 5 months of age (*55*). In previous studies, degenerative changes of the adult tendon and enthesis in response to increased loading include increased cross-sectional area (CSA) (*29*), higher cellularity (*49*, *51*), neovascularization (*49*), and reduced fiber organization (*29*, *49*, *51*). Excessive repeated loading can also lead to reduced stiffness and strength (*52*). However, in our study, repeated muscle-induced loading of the adult enthesis did not lead to pathological adaptation. This could be a result of physiological and isometric loading or post-loading compensatory recovery after dosing.

Increased and repeated loading leads to dose-dependent degeneration in tendon and enthesis by the accumulation of subfailure damage. Collagen is the primary stabilizing constituent of the tendon, bone, and enthesis ECM and the key contributing factor

Downloaded from https://www.science.org on July 08, 2024

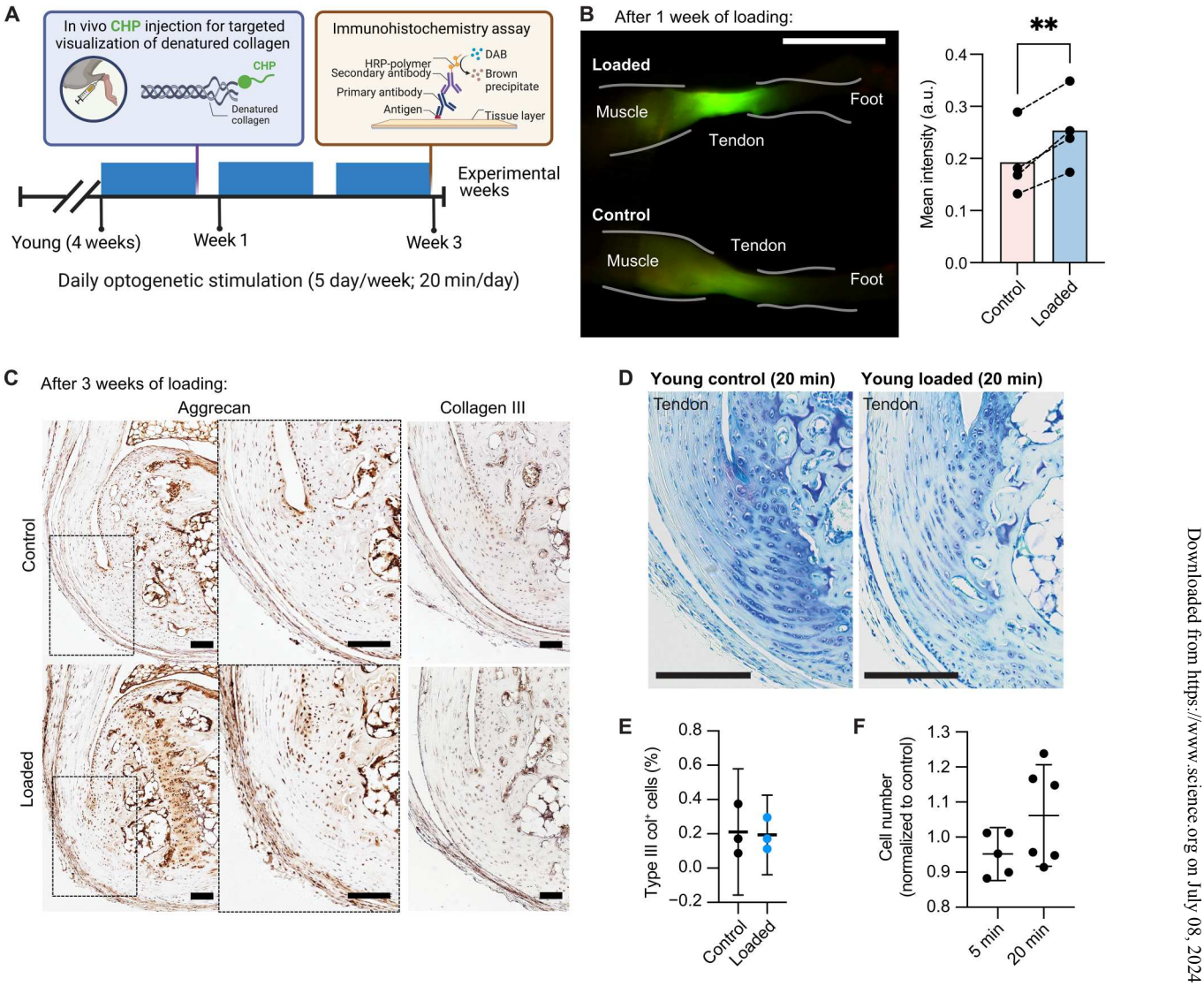

Fig. 4. Repeated loading led to denatured collagen fibers and increased prevalence of ECM components at the enthesis and growth plate. (**A**) Schematic shows the experimental design for evaluation of the effect of repeated loading on ECM of the young tendon and enthesis. HRP, horseradish peroxidase. DAB, 3,3′-Diaminobenzidine. (**B**) Repeated loading resulted in the accumulation of collagen denaturation in loaded tendon and enthesis. Data were compared using paired *t* test (two-tailed; assuming Gaussian distribution, parametric; $^{**}P = 0.0062$. a.u., arbitrary units. (**C** and **E**) Loaded entheses did not exhibit differences in localized aggrecan or type III collagen at the enthesis compared to controls. Type III collagen cell count data were compared using unpaired *t* tests (nonparametric; Mann-Whitney test; two-tailed; $P > 0.9999$). (**D**) However, loading qualitatively influenced the pericellular matrix and cell shape, but not cell number, at the enthesis in young mice. (**F**) Cell number was not affected by the duration of loading (5 min versus 20 min; unpaired nonparametric *t* test; Mann-Whitney, two-tailed; $P = 0.1342$). Scale bars, (B) 10 mm and (C) and (D) 100 μm. Error bars denote mean ± 95% confidence interval. Created with BioRender.com.

to the elastic behavior of the tendon (*58*) and toughness of the bone (*59*). In the tendon, structural reorganization of collagen fibers can be exacerbated into nonreversible molecular level denaturation of the collagen fiber collagen, ultimately leading to inferior mechanical properties (*46*). CHPs are synthetic single-strand peptides that have recently been developed to hybridize with denatured collagen triple helix. In tendon, CHPs can specifically bind to nonrecoverable (post-yield) sites of collagen fibril unfolding (*27*, *46*). Enzymatic and mechanical factors drive tendon ECM degradation and remodeling processes (*60*). In the present study, we found that repeated loading did not result in the up-regulation of genes associated with matrix metalloproteinases, rather, loading down-regulated *Mmp9* and several other genes associated with ECM remodeling. These findings suggest that the increased in vivo labeling of the Achilles tendon with CHPs may be caused by increased collagen denaturation, and not enzymatic degradation. Similar to findings from repeatedly loaded tendon ex vivo (*61*), our results show that loading-induced collagen denaturation does not coincide with altered tissue stiffness. These findings suggest a compensatory mechanism (e.g., collagen fiber sliding) rather than a fiber-dominant pre-yield mechanism of load transfer in the tendon and enthesis. Alternatively, repeated loading in growing enthesis leads to reduced mineral deposition at subchondral and apophyseal bone and disruption of ECM composition in young enthesis that

Downloaded from https://www.science.org on July 08, 2024

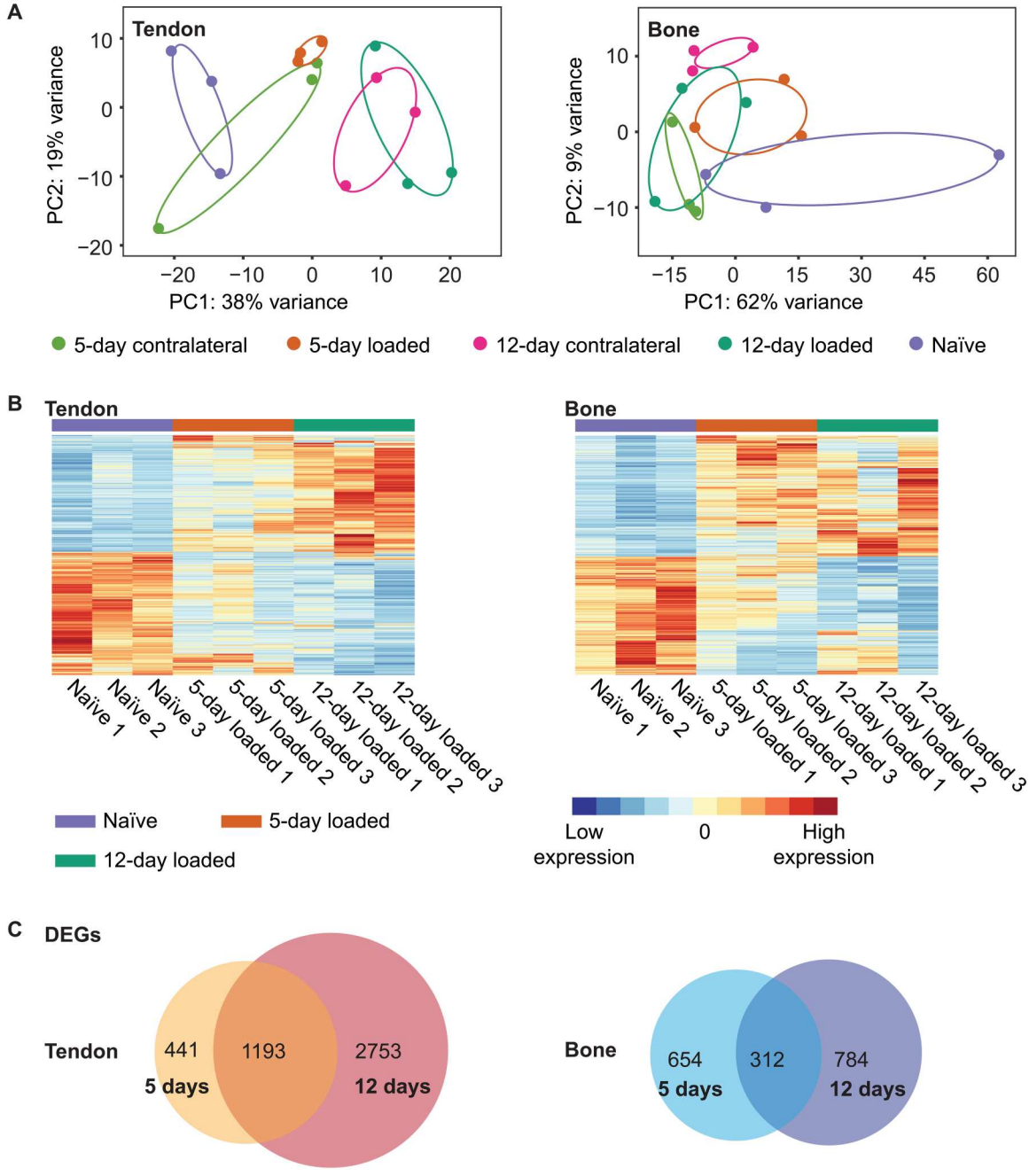

Fig. 5. Optogenetic-induced loading led to transcriptional response in both tendon and bone. (**A**) Principal component (PC) analysis plots of differential gene expression for naïve, contralateral, and loaded tendons and bones after 5 and 12 days of loading. (**B**) Heatmaps of all DEGs for Achilles tendon and calcaneus (bone) in naïve, 5-day loaded, and 12-day loaded mice. (**C**) In tendon and bone 1193 and 312 genes, respectively, were differentially expressed after 5 and 12 days of loading. DEGs were identified using Wald test in R/Bioconductor/DESeq2 with Benjamini-Hochberg *P*-adj < 0.05. *N* = 15 per tissue.

functionally translate to significant decrease of enthesis toughness and tensile strength. These results are in agreement with the role of mineral as the primary toughening constituent of the enthesis (*4*).

The ECM disruption and altered calcaneal shape in the Young-loaded calcaneus suggest an unexplored role of mechanical loading in enthesis and apophysis adaptation during growth. The role of increased loading on the formation and maturation of the mineralizing growth plate during postnatal maturation was elucidated in our bulk RNA-seq studies, and we identified key pathways that are transcriptionally activated in the growing calcaneus and tendon. We observed down-regulation of genes associated with mechanosensitive pathways and processes, such as ECM-receptor interaction, focal adhesion, etc. Overuse of tendon can disrupt mechanotransduction by altering cell signaling structures and the surrounding matrix environment (*62*). Type VI collagen and type II fibrillin, two major constituents of the tenocyte pericellular matrix (*63*), were

Downloaded from https://www.science.org on July 08, 2024

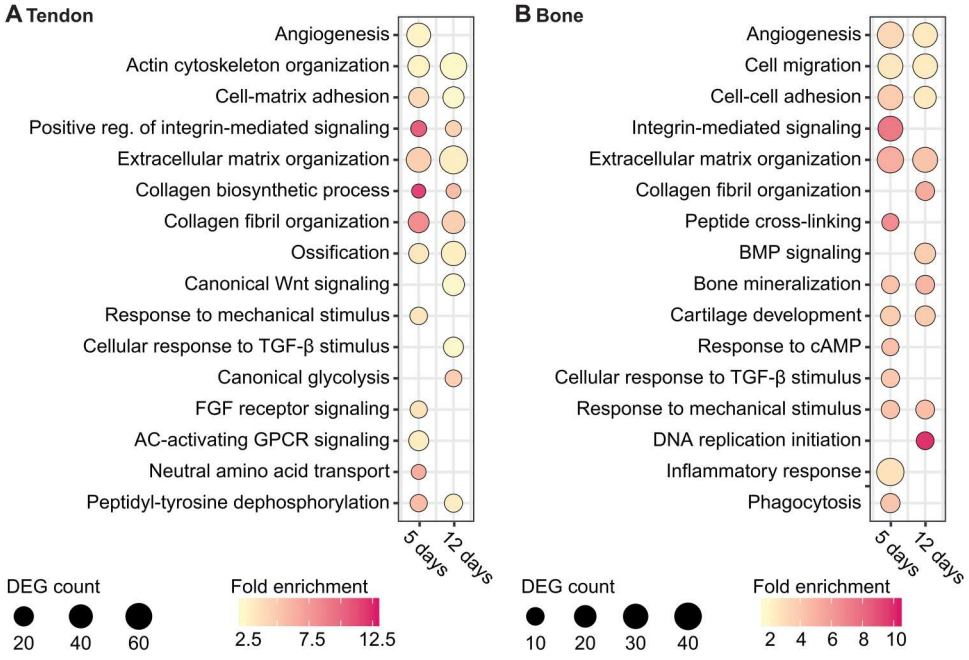

Fig. 6. Relevant biological processes that were differentially regulated by optogenetically induced loading in young Achilles tendon and bone (calcaneus). Increased muscle loading on (**A**) tendon and (**B**) bone resulted in enrichment of key biological processes, such as angiogenesis, integrin-mediated signaling, and extracellular matrix organization, at one or both time points. Loading enriched processes related to cell adhesion, cytoskeleton and ECM regulation, mechanotransduction, and ossification in both tissues. Biological processes were identified using DAVID's statistical test of overrepresentation with false discovery rate (FDR) < 0.05 and enrichment > 1.5. TGF-β, transforming growth factor–β; FGF, fibroblast growth factor; GPCR, G protein–coupled receptor; AC, adenylyl cyclase; BMP, bone morphogenetic protein; cAMP, cyclic adenosine monophosphate.

consistently down-regulated with loading, indicating that tendon overloading and associated ECM disruption may have compromised the interaction between the cell and ECM (*62*, *64*). Sun *et al.* (*65*) showed that the expression of integrins in tendon did not correlate with the increase of loading dose, suggesting an overuse-induced ECM damage that regulates mechanosensitivity. Our findings model the structural and mechanical changes similar to those occurring in pediatric apophyseal pathologies and in young athletes (*66*, *67*). This study provides the first small animal model of pediatric apophyseal pathologies and can be leveraged for future systematic examination of mechanisms of injury and repair in the growing skeleton. Establishing the time course of gene expression of mechanosensitive pathways following loading and during key periods of remodeling will be important next steps for future studies.

Although muscle contraction was confirmed throughout the experimental loading duration, the translated loads from muscle to tendon, enthesis, and bone during loading are unknown. Berman *et al.* (*68*) showed that comparable ankle torques to what we measured can induce osteogenic strains in the tibial mid-diaphysis in adult mice. In addition, step cycle and triceps surae activation durations were previously reported as approximately 300 to 400 ms in adult C57BL6J mice (*69*, *70*). In this study, we have used optical stimulation at supraphysiological duration of 1000 ms and 10-Hz optical cell activation frequency, which is within and in the lower range of motor unit frequencies in the triceps surae muscle in adult mice (*71*). Future studies should investigate ways to improve transgenic strains for sustained contractile fusion using optogenetic stimulation. Last, there may be unknown physiological changes that directly or indirectly affect the mechanoadaptation of the tendon and enthesis.

In summary, this work provides an understanding of enthesis and calcaneal bone adaptation to mechanical loading, induced by optogenetic control of skeletal muscle contraction. This useful tool to control tendon, enthesis, and bone loading is advantageous for understanding the mechanobiology of the immature musculoskeleton that provides an easily translatable approach to other anatomical sites.

MATERIALS AND METHODS

All procedures were approved by the Institutional Animal Care and Use Committees at the University of Delaware (AUP 1296) and the University of Michigan (PRO00009507). Doxycycline-inducible ACTA1-rtTA;tetO-cre mice (Acta1-Cre; C57BL6J background; Jackson Lab ID: 012433) and Ai32 reporter mice (Jax ID: 024109, C57BL6J background) were obtained from the Jackson Laboratory (Bar Harbor, ME, USA). Acta1-Cre and Ai32 reporter mice were bred to generate F2 (Ai32 homozygous) lines that expressed a yellow fluorescent protein (YFP)–fused *ChR2* light-sensitive opsin (455-nm sensitivity) in skeletal muscle when treated with tetracycline. Dams were treated with doxycycline chow at the time of mating and maintained on chow until offspring were weaned. Previously, we have shown that the muscle-specific and nerve-independent expression of ChR2-EYFP is maintained in adult mice (up to 6-month-old offspring) when treated with doxycycline during gestation and before weaning only (*44*). Offspring were genotyped using PCR (Transnetyx, Cordova, TN, USA). A total of 57 mice

Downloaded from https://www.science.org on July 08, 2024

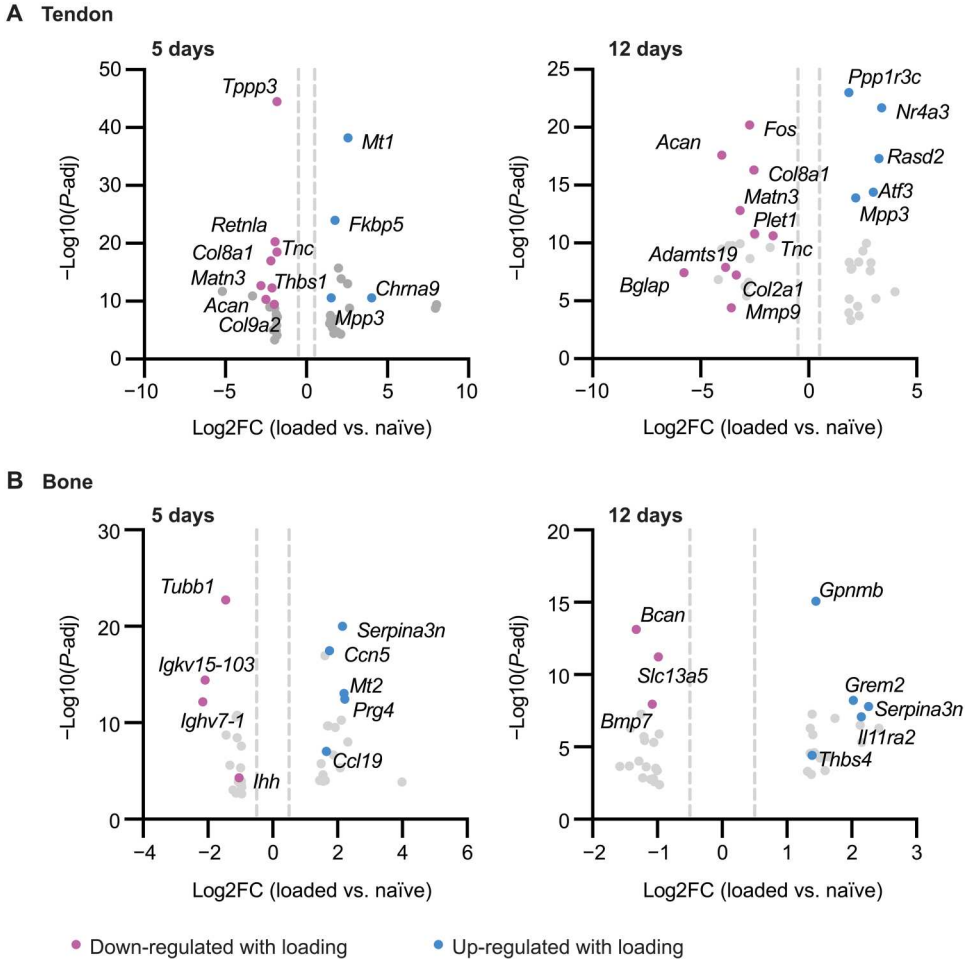

Fig. 7. After 5 days and 12 days of stimulation, daily bouts of optogenetic loading led to significant down-regulation of genes associated with tendon stem cell activation and ECM synthesis in tendon and up-regulation of proinflammatory markers in bone. Data shown are $\log_2$-transformed fold change (log2FC, *x* axis) and $-\log_{10}$ transformed *P*-adj (−log10(*P*-adj), *y* axis) for (**A**) tendon and (**B**) bone. Dashed lines denote ±0.5 log2FC.

were used in this study. Mice were randomized across various experiments. ActaCre;Ai32 homozygous mice (n = 38 total) were used for unilateral light-induced stimulation of muscle in young (3 to 4 weeks old, n = 30; 12 females and 18 males) or adult (6 to 8 months old, n = 8; 2 females and 6 males) mice. Contralateral (within-animal) limbs were used as paired controls. In addition, a second group of ActaCre;Ai32 mice was used to compare age-matched littermates as naïve controls for both young (n = 11; five females and six males) and adult (n = 4; two females and two males) groups (Fig. 7). An additional 3-month-old ActaCre;Ai32 mouse was used to test muscle contractility response to blue light in vitro. Unless otherwise stated, all animals were included for the respective analyses described below.

Optogenetics stimulation for daily tendon enthesis loading

Mice were anesthetized with isoflurane, and hair was removed using chemical hair remover from their right triceps surae muscles (Nair, Church and Dwight, Ewing, NJ, USA). Animals were placed on a heating pad in the prone position, and body temperature was maintained at 37°C (Stoeling, Wooddale, Il, USA). The right limb was stabilized at the knee joint with a clamp, and the right foot was placed on a foot pedal for isometric muscle stimulation. Animals were weighed daily before stimulations. For light stimulation, a collimated LED light (455 nm, 900 mW, M455L3, Thorlabs) and a high-power LED driver (DC2200, Thorlabs, Newton, NJ) were used for pulse modulation (*44*). Driver code was adjusted in LabView (National Instruments, Austin, TX, USA) to add pulsatile light activation and deactivation controls (bouts of stimulation and rest) for the period of experiment. Light source was placed above the triceps surae muscles at a distance to induce a light intensity of ~0.3 mW/mm^2. Triceps surae muscles were stimulated using an approximated 10-Hz pulsed light (70 ms on, 30 ms off; 10 cycles) followed by 4 s of rest for 20 min (240 consecutive loading cycles) in young (n = 27, 12 females and 15 males) and adult (n = 8, 2 females and 6 males) groups. Daily bouts of loading were repeated weekly with 5 days of stimulation and 2 days of rest for up to 3 weeks (19 days). A subset of these mice in the young group (n = 7) was also used to measure ankle torque throughout the stimulation using a servomotor shaft (Aurora 3-in-1 system, Aurora Scientific, Ontario, Canada) that was connected to the foot pedal. All other mice were loaded in a three-dimensional (3D) printed mimic of the platform. Knee and ankle placements were replicated for the

Downloaded from https://www.science.org on July 08, 2024

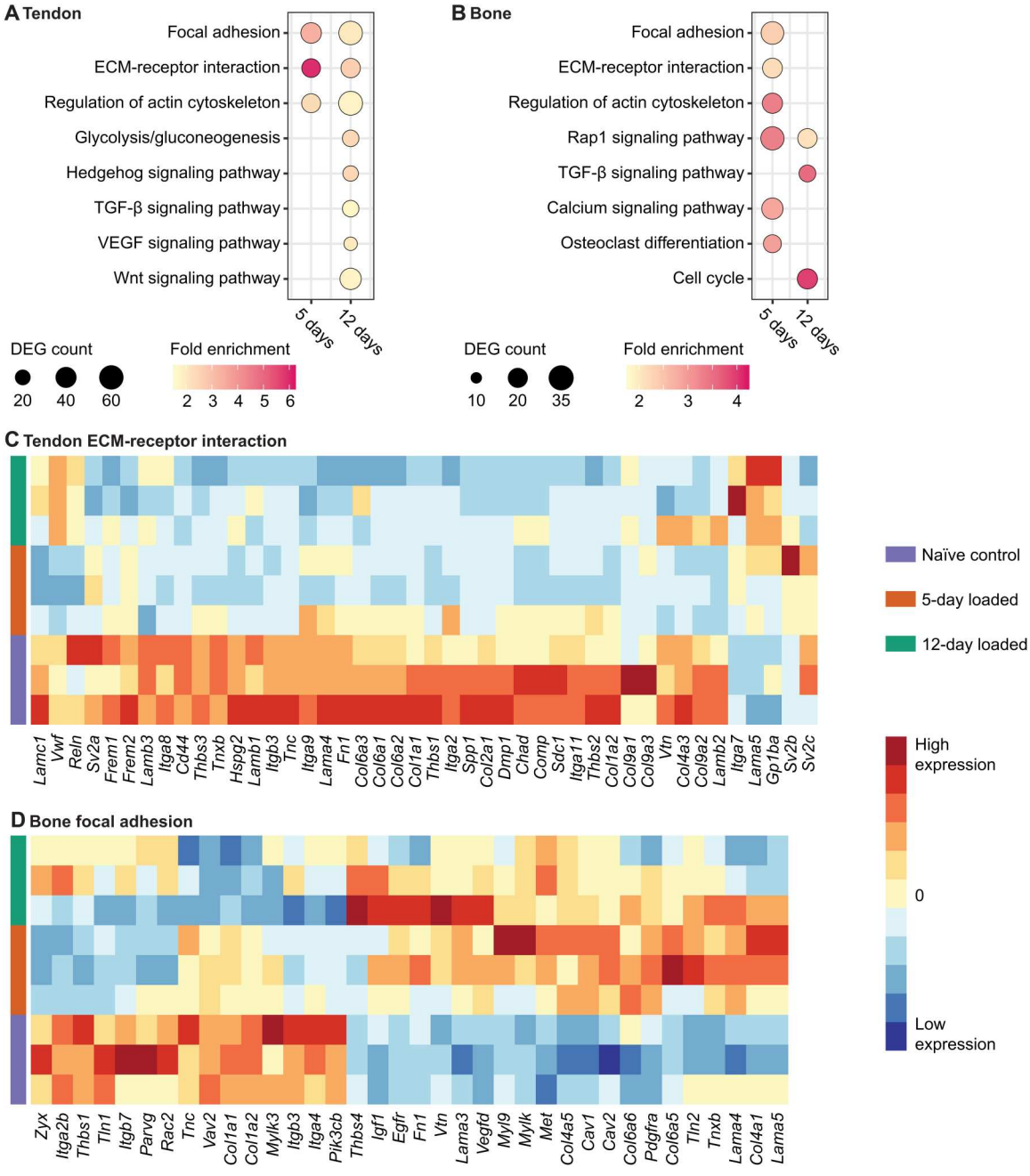

Fig. 8. Relevant KEGG pathways that were differentially regulated by optogenetics-induced loading in Young Achilles tendon and bone (calcaneus). Enriched KEGG pathways, including mechanobiological pathways such as ECM-receptor interaction and focal adhesion, were identified in both (**A**) tendon and (**B**) bone at one or both time points. (**C**) ECM-receptor interaction pathway in tendon is driven by 44 genes of which >90% are down-regulated with loading, while in (**D**) calcaneus focal adhesion pathway is driven by 36 genes of which >50% are up-regulated with loading. Pathways were identified using DAVID's statistical test of overrepresentation with an FDR < 0.05 and enrichment > 1.5. VEGF, vascular endothelial growth factor.

young control group for 20 min daily under anesthesia. After recovery from anesthesia, mice were returned to their cages for unrestricted cage activity. An additional cohort of young mice was added to compare the effects of bout duration (5 min "short" loading; 60 consecutive cycles; $n = 5$, two females and three males) loading duration on weight gain over the 3-week duration of the experiment.

In vitro contractility with optogenetic stimulation

Right EDL muscles were dissected from 3-month-old ActaCre;Ai32 mice (doxycycline removed at 3 weeks of age) and were placed in a buffered Ringer's solution bath. Distal and proximal tendons of EDL were tied with sutures to a fixed post and force transducer (BG-50, Kulite Semiconductor), respectively (*72*). Blue light (455-nm LED; ~140 mW/cm2; Thorlabs) was shone on the muscle to

Downloaded from https://www.science.org on July 08, 2024

evoke optogenetic twitches. Forces were recorded with and incremental light pulse duration ranging from 5 to 70 ms.

Micro-computed tomography

Mice were euthanized using carbon dioxide asphyxiation 48 hours after the final bout of loading. The skin was carefully dissected, and distal hindlimbs (knee, ankle, and foot) were fixed for 24 hours in 4% paraformaldehyde. Calcaneus-tibial complexes were scanned using micro–computed tomography (microCT) at the University of Delaware (microCT, Bruker SkyScan 1276; 59 kV, 175 μA, 10.58-μm voxel size, 930-ms exposure, 0.5-mm aluminum filter).

Bone morphometry and statistical shape modeling

Aligned image stacks were reconstructed at the University of Michigan for qualitative and quantitative assessment of calcaneal bone shape using Dragonfly software (v2022.2, Object Research Systems, Montreal, Quebec). After reconstruction, the calcaneus was aligned vertically along its long axis and transversely cropped to include the peroneal tubercle. Bone morphometry was assessed within this volume after applying a median filter in 3D (square median kernel size =3) and "split at Otsu" to identify bone and non-bone regions. We then calculated TV BV, and BV/TV for bone morphometry. To generate solid objects for use in statistical shape modeling, we digitally cleaned the regions of interest (ROIs) to remove other bones and filled the growth plate and trabecular/marrow cavities (complete fill) in Dragonfly. ROIs from left (control) image datasets were mirrored to anatomically mimic right (loaded) image datasets for shape modeling. We then created a mesh and imported STL files into ShapeWorks Studio (6.3.2; http://shapeworks.sci.utah.edu). Shapes were groomed to fill holes, smoothened (Laplacian, 10 iterations, relaxation = 1), remeshed (75% number of vertices and 1.00 adaptivity), and aligned (based on three anatomical landmarks at processes of the calcaneal tuberosity). Optimization was performed using the following settings: number of particles = 512; initial relative weighting = 1; relative weighting = 200; starting/ending regularization = 1000; iterations per split = 1000; optimization iterations = 1000; Procrustes rotation/translation = yes; Procrustes interval = 10; and narrow band = 4. Quality was assessed via metrics (compactness, specificity, and generalization) for shape modes, and principal component analyses were evaluated for young shapes only (control versus loaded) because of the limited sample size in the Adult group. Deformation maps were generated to visualize shape changes from the mean shape of the control group to the mean shape of the loaded group, with growth or loss in response to loading shown in red or blue, respectively. Comparisons were made between young (loading started at 4 weeks of age; control and loaded) samples from 20-min bouts (3-week duration; n = 7 control and n = 7 loaded) and between adult (control and loaded) samples from 20-min bouts (3-week duration; n = 4 control and n = 4 loaded). Because of the low sample size (n = 4), statistical shape analyses were not performed on adult mice.

Table 1. Antigen retrieval and antibody information for immunohistochemistry experiments. IgG, immunoglobulin G.

Antibody	Source and catalog #	Dilution	Buffer; antigen retrieval
Anti-collagen III(rabbit polyclonal)	Abcam, ab7778	1:100	Tris-EDTA (pH 9.0), 65°C, 2 hours
Anti-aggrecan (rabbit polyclonal)	Abcam, ab216965	1:100	0.1% trypsin, 37°C, 30 min
Biotinylated goat anti-mouse IgG	MilliporeSigma, 20777	1:1000	Room temperature, 10 min
Biotinylated goat anti-rabbit IgG	MilliporeSigma, 20715	1:1000	Room temperature, 10 min
Primer	Version	Company	Assay ID
Tnc	PrimeTime qPCR primers	IDT	Mm.PT.58.8090418
Col1a1	PrimeTime qPCR primers	IDT	Mm.PT.58.7562513
Col1a2	PrimeTime qPCR primers	IDT	Mm.PT.58.5206680
Col2a1	PrimeTime qPCR primers	IDT	Mm.PT.58.10123677
B2m	PrimeTime qPCR primers	IDT	Mm.PT.39a.22214835

Histology

Distal hindlimbs from mice treated with 20-min of loading for 3 weeks (19 days) as well as from naïve controls were decalcified in 14% EDTA and processed for paraffin embedding. Tissues were sectioned at 6 μm in the sagittal plane and stained with hematoxylin and eosin or Toluidine blue and coverslipped with an acrylic mounting media (Acrymount, StatLab, McKinnery, TX, USA) or used for immunohistochemistry. For immunohistochemistry, paraffin sections were deparaffinized and quenched in 0.3% hydrogen peroxide (Santa Cruz Biotechnology, Dallas, TX), followed by heat-mediated antigen retrieval and blocking (5% goat serum in phosphate buffer saline). Slides were then incubated in primary antibodies (listed in Table 1) overnight at 4°C, followed by washing and incubation with appropriate secondary antibodies. Horseradish peroxidase 3,3′-diaminobenzidine system (MilliporeSigma, Billerica, MA, USA) was used for detection, and slides were counterstained with hematoxylin and coverslipped with Acrymount (Acrymount, StatLab, McKinney, TX, USA). All slides were imaged on a bright-field microscope (ECLIPSE Ni-U, Nikon).

Biomechanical testing of the Achilles enthesis

After 3 weeks of daily (20 min; five consecutive days per week) loading, young and adult mice were euthanized, and carcasses were stored intact at −20°C until testing. Carcasses were thawed at 4°C for no more than 24 hours, and Achilles tendon-calcaneus complex was carefully dissected and stored in phosphate-buffered saline (PBS) for no more than 2 hours at room temperature. Before mechanical testing, the muscle was carefully dissected from the Achilles tendon, the plantaris tendon was detached, and the calcaneus was disarticulated from the foot. CSA measurements were made using photogrammetry with a custom 3D printed fixture attached to a motor controller (Arduino, Ivrea, Italy). Forty consecutive images of the tendon-bone complex were acquired at 9°

Downloaded from https://www.science.org on July 08, 2024

rotation steps using a macro lens (Basler Fujinon Lens, Ahrensburg, Germany). Images were converted from sparse to dense point clouds, and an STL surface mesh of the tendon was generated using Metashape software (Agisoft, St. Petersburg, Russia). CSA was measured using Dragonfly software at the Achilles tendon near the enthesis. The calcaneus was then placed in a custom 3D printed fixture to secure the bone (FormLabs 3B, Somerville, MA, USA), and the proximal Achilles tendon was clamped in a thin film grip (Imada, Northbrook, IL, USA) (*73*). The assembled tendon-grip unit was placed in a custom PBS bath maintained at 37°C via a temperature controller (MA160, Biomomentum Inc., Laval, Quebec, Canada) and secured with a pin to a tensile testing frame with multi-axis load cells (±70 N; Mach-1 VS500CST, Biomomentum, Laval, Quebec, Canada). Samples were preloaded to 0.01 N, and gauge length (L_0) was measured (4.01 ± 0.17 mm) as the distance between the calcaneal fixture and the thin film grip. Tendons were preconditioned for 10 cycles (±0.05 N at 0.03 Hz) followed by load to failure at 0.05 mm/s. Load and torque data (six degrees of freedom) were collected to assess off-axis loading for the duration of the experiment. Using Mach-1 Analysis and custom MATLAB script (R2017 or later, MathWorks, Natick, USA), the mechanical properties of the entheses were calculated from force-displacement data. Engineering stress was calculated as the instantaneous force divided by the original CSA (calculated from photogrammetry). Instantaneous grip-to-grip strain was calculated as the displacement divided by the original gauge length, L_0. Stiffness and elastic modulus were calculated from the linear portion of the load-displacement and stress-strain curves, respectively. Maximum load, maximum stress, and maximum strain were calculated, as well as work to maximum force (area under the curve) and toughness from the area under the force-displacement and stress-strain curves. Maximum strain was calculated as the strain at maximum force.

Collagen hybridization and damage visualization

Young mice were loaded for 20 min daily for 5 days ($n = 4$). Immediately following the last bout of loading, 20 μl of sulfo-Cy7.5 CHP (3Helix, Salt Lake City, UT, USA) was injected subcutaneously adjacent to the Achilles tendon mid-substance using an insulin syringe (Exel International, CA, USA). Mice were imaged under anesthesia (85-μm pixel resolution; 700- and 800-nm wavelength; Li-Cor Pearl imager) 24 hours after the injection. Intensity measurements were taken in a user-defined ROI at the Achilles tendon and enthesis using Li-Cor image acquisition software for both 700- and 800-nm wavelengths.

RNA-seq of tendon and bone

Young mice were euthanized 4 hours after the 5th or 12th consecutive day of loading, and tendon and calcaneal bone from loaded and contralateral (not loaded) limbs were immediately dissected under ribonuclease (RNase)–free conditions and snap-frozen (n = 3 male mice per time point). Age-matched Achilles tendons and calcaneal bones were also collected as a naïve control group ($n = 3$ male mice; age matched to the fifth consecutive day time point). Tissues were mechanically pulverized in TRIzol, and total RNA was isolated using spin-columns (PureLink RNA mini kit, Thermo Fisher Scientific) with on column genomic DNA digestion (RNase-free DNase, QIAGEN). RNA Integrity Number (RIN) was measured using Bioanalyzer (Agilent). Poly-A mRNA libraries were prepared, and next-generation sequencing was performed using Illumina NovaSeq shared platform. Reads were mapped to the genome reference consortium mouse build 38. Differential gene expression was determined from count matrices with either paired design (loaded versus contralateral) or unpaired design (loaded or contralateral versus naïve control) in DESeq2 in R/Bioconductor (*74*).

Gene expression verification with qRT-PCR

We verified gene expression of four genes that were differentially expressed in tendon with loading: *Tnc*, *Col1a1*, *Col1a2*, and *Col2a1* (Integrated DNA Technologies) with qRT-PCR. Redundant RNA following sequencing from naïve, 5-day loaded, and 12-day loaded samples (n = 3 per group) was reverse-transcribed to cDNA (SuperScript IV VILO Master Mix, Thermo Fisher Scientific). The quality and quantity of RNA were checked with a NanoDrop spectrophotometer (Thermo Fisher Scientific) before conversion. qRT-PCR was performed in CFX96 Real-Time PCR Detection System (Bio-Rad) with Power SYBR Green PCR Master Mix (Thermo Fisher Scientific). *B2m* was used as the reference gene. Primer information is provided in Table 1.

Statistical analysis

Statistical comparisons were performed using Prism (8.3 or higher, GraphPad Software, La Jolla, USA) or in R (version 4.1.0). Gaussian distribution of the data was evaluated using Shapiro-Walik and D′Agostino-Pearson normality tests. Results from microCT analyses were tested for normality and compared between the loaded and control samples using an unpaired t tests. For statistical comparison of the CSA measurements and mechanical testing results, parametric data were tested using paired two-tailed t test, and Wilcoxon rank test was used for nonparametric results. To identify DEGs, we used Wald test of significance and corrected P values for multiple testing using the Benjamini and Hochberg method (P-adj < 0.05). Log2FCs were shrunk to account for high dispersion and low counts (*75*). The median ratio algorithm of DESeq2 was used to normalize counts for sequencing depth and gene length (*76*). For functional annotation, list of DEGs with $|\log2FC| \geq 0.32$ was input separately for each time point and tissue into DAVID (*77*, *78*) with *Mus musculus* background. Gene Ontology biological processes and KEGG pathways were obtained with a false discovery rate < 0.05 and fold enrichment ≥ 1.5. For power analysis, the effect size was calculated from the descriptive statistics of each group, and the effect size was calculated as the ratio of mean and SD of difference. Power for each variable was calculated using total sample size (N = 16), significance ($\alpha = 0.05$), and the calculated effect size for a t test with match mean values. For power < 0.8, a priori power analysis was performed to calculate the required sample size to achieve 0.8 power. For most outcomes, statistical significance was considered as P = or < 0.05. Means ± SD are reported. All images were deidentified and analyzed by at least one blinded reviewer, and results were aggregated by one of the lead authors (S.N.L., E.G., or M.L.K.) for sorting.

Supplementary Materials

This PDF file includes:

Figs. S1 and S2
Table S1
Legend for data S1

Downloaded from https://www.science.org on July 08, 2024

Other Supplementary Material for this manuscript includes the following:
Data S1

View/request a protocol for this paper from *Bio-protocol*.

REFERENCES AND NOTES

1. L. Rossetti, L. A. Kuntz, E. Kunold, J. Schock, K. W. Müller, H. Grabmayr, J. Stolberg-Stolberg, F. Pfeiffer, S. A. Sieber, R. Burgkart, A. R. Bausch, The microstructure and micromechanics of the tendon–bone insertion. *Nat. Mater.* **16**, 664–670 (2017).
2. M. Benjamin, D. McGonagle, "The entheisis organ concept and its relevance to the spondyloarthropathies" in *Molecular Mechanisms of Spondyloarthropathies*, C. López-Larrea, R. Díaz-Peña, Eds. (Springer, 2009), pp. 57–70.
3. S. Thomopoulos, J. P. Marquez, B. Weinberger, V. Birman, G. M. Genin, Collagen fiber orientation at the tendon to bone insertion and its influence on stress concentrations. *J. Biomech.* **39**, 1842–1851 (2006).
4. M. Golman, A. C. Abraham, I. Kurtaliaj, B. P. Marshall, Y. J. Hu, A. G. Schwartz, X. E. Guo, V. Birman, P. J. Thurner, G. M. Genin, S. Thomopoulos, Toughening mechanisms for the attachment of architectured materials: The mechanics of the tendon entheisis. *Sci. Adv.* **7**, eabi5584 (2021).
5. G. M. Genin, S. Thomopoulos, Unification through disarray. *Nat. Mater.* **16**, 607–608 (2017).
6. J. M. Weatherall, K. Mroczek, N. Tejwani, Acute achilles tendon ruptures. *Orthopedics* **33**, 758–764 (2010).
7. J. A. Ogden, T. M. Ganey, J. D. Hill, J. I. Jaakkola, Sever's injury: A stress fracture of the immature calcaneal metaphysis. *J. Pediatr. Orthop.* **24**, 488–492 (2004).
8. M. M. Duong, A. D. Nicholson, S. Q. Li, A. Gilmore, D. R. Cooperman, R. W. Liu, Relationship between sever disease and skeletal maturity. *J. Pediatr. Orthop.* **40**, 93–96 (2020).
9. M. Benjamin, H. Toumi, J. R. Ralphs, G. Bydder, T. M. Best, S. Milz, Where tendons and ligaments meet bone: Attachment sites ('entheses') in relation to exercise and/or mechanical load. *J. Anat.* **208**, 471–490 (2006).
10. N. Maffulli, J. Wong, L. C. Almekinders, Types and epidemiology of tendinopathy. *Clin. Sports Med.* **22**, 675–692 (2003).
11. C. E. Shopfner, C. G. Coin, Effect of weight-bearing on the appearance and development of the secondary calcaneal epiphysis. *Radiology* **86**, 201–206 (1966).
12. M. Kvist, Achilles tendon injuries in athletes. *Ann. Chir. Gynaecol.* **80**, 188–201 (1991).
13. J. I. Wiegerinck, R. Zwiers, I. N. Sierevelt, H. C. P. M. van Weert, C. N. van Dijk, P. A. A. Struijs, Treatment of calcaneal apophysitis: Wait and see versus orthotic device versus physical therapy: A pragmatic therapeutic randomized clinical trial. *J. Pediatr. Orthop.* **36**, 152–157 (2016).
14. A. Schwartz, J. H. Lipner, J. D. Pasteris, G. M. Genin, S. Thomopoulos, Muscle loading is necessary for the formation of a functional tendon entheisis. *Bone* **55**, 44–51 (2013).
15. M. L. Killian, S. Thomopoulos, Scleraxis is required for the development of a functional tendon entheisis. *FASEB J.* **30**, 301–311 (2016).
16. M. L. Killian, Growth and mechanobiology of the tendon-bone entheisis. *Semin. Cell Dev. Biol.* **123**, 64–73 (2022).
17. E. Blitz, S. Viukov, A. Sharir, Y. Shwartz, J. L. Galloway, B. A. Pryce, R. L. Johnson, C. J. Tabin, R. Schweitzer, E. Zelzer, Bone ridge patterning during musculoskeletal assembly is mediated through SCX regulation of Bmp4 at the tendon-skeleton junction. *Dev. Cell* **17**, 861–873 (2009).
18. H. M. Shaw, M. Benjamin, Structure-function relationships of entheses in relation to mechanical load and exercise. *Scand. J. Med. Sci. Sports* **17**, 303–315 (2007).
19. J. Kahn, Y. Shwartz, E. Blitz, S. Krief, A. Sharir, D. A. Breitel, R. Rattenbach, F. Relaix, P. Maire, R. B. Rountree, D. M. Kingsley, E. Zelzer, Muscle contraction is necessary to maintain joint progenitor cell fate. *Dev. Cell* **16**, 734–743 (2009).
20. I. Rot-Nikcevic, T. Reddy, K. J. Downing, A. C. Belliveau, B. Hallgrímsson, B. K. Hall, B. Kablar, Myf5 −/− :MyoD −/− amyogenic fetuses reveal the importance of early contraction and static loading by striated muscle in mouse skeletogenesis. *Dev. Genes Evol.* **216**, 1–9 (2006).
21. S. Achar, J. Yamanaka, Apophysitis and osteochondrosis: Common causes of pain in growing bones. *Am. Fam. Physician* **99**, 610–618 (2019).
22. M. E. Lynch, R. P. Main, Q. Xu, D. J. Walsh, M. B. Schaffler, T. M. Wright, M. C. H. van der Meulen, Cancellous bone adaptation to tibial compression is not sex dependent in growing mice. *J. Appl. Physiol.* **109**, 685–691 (2010).
23. R. L. De Souza, M. Matsuura, F. Eckstein, S. C. F. Rawlinson, L. E. Lanyon, A. A. Pitsillides, Non-invasive axial loading of mouse tibiae increases cortical bone formation and modifies trabecular organization: A new model to study cortical and cancellous compartments in a single loaded element. *Bone* **37**, 810–818 (2005).
24. T. K. Patel, M. D. Brodt, M. J. Silva, Experimental and finite element analysis of strains induced by axial tibial compression in young-adult and old female C57Bl/6 mice. *J. Biomech.* **47**, 451–457 (2014).
25. S. P. Kotha, Y.-F. Hsieh, R. M. Strigel, R. Müller, M. J. Silva, Experimental and finite element analysis of the rat ulnar loading model—Correlations between strain and bone formation following fatigue loading. *J. Biomech.* **37**, 541–548 (2004).
26. A. G. Robling, F. M. Hinant, D. B. Burr, C. H. Turner, Improved bone structure and strength after long-term mechanical loading is greatest if loading is separated into short bouts. *J. Bone Miner. Res.* **17**, 1545–1554 (2002).
27. D. T. Fung, V. M. Wang, N. Andarawis-Puri, J. Basta-Pljakic, Y. Li, D. M. Laudier, H. B. Sun, K. J. Jepsen, M. B. Schaffler, E. L. Flatow, Early response to tendon fatigue damage accumulation in a novel in vivo model. *J. Biomech.* **43**, 274–279 (2010).
28. J. B. Sereysky, N. Andarawis-Puri, K. J. Jepsen, E. L. Flatow, Structural and mechanical effects of in vivo fatigue damage induction on murine tendon. *J. Orthop. Res.* **30**, 965–972 (2012).
29. L. J. Soslowsky, S. Thomopoulos, S. Tun, C. L. Flanagan, C. C. Keefer, J. Mastaw, J. E. Carpenter, Neer Award 1999: Overuse activity injures the supraspinatus tendon in an animal model: A histologic and biomechanical study. *J. Shoulder Elbow Surg.* **9**, 79–84 (2000).
30. A. C. Abraham, S. A. Shah, M. Golman, L. Song, X. Li, I. Kurtaliaj, M. Akbar, N. L. Millar, Y. Abu-Amer, L. M. Galatz, S. Thomopoulos, Targeting the NF-κB signaling pathway in chronic tendon disease. *Sci. Transl. Med.* **11**, eaav4319 (2019).
31. B. P. Thampatty, J. H.-C. Wang, Mechanobiology of young and aging tendons: In vivo studies with treadmill running. *J. Orthop. Res.* **36**, 557–565 (2018).
32. A. C. Abraham, F. Fang, M. Golman, P. Oikonomou, S. Thomopoulos, The role of loading in murine models of rotator cuff disease. *J. Orthop. Res.* **40**, 977–986 (2022).
33. Y. J. Kim, H. J. Kim, W. J. Lee, J. K. Seong, A comparison of the metabolic effects of treadmill and wheel running exercise in mouse model. *Lab. Anim. Res.* **36**, 3 (2020).
34. I. Lerman, B. C. Harrison, K. Freeman, T. E. Hewett, D. L. Allen, J. Robbins, L. A. Leinwand, Genetic variability in forced and voluntary endurance exercise performance in seven inbred mouse strains. *J. Appl. Physiol.* **92**, 2245–2255 (2002).
35. M. Svensson, P. Rosvall, A. Boza-Serrano, E. Andersson, J. Lexell, T. Deierborg, Forced treadmill exercise can induce stress and increase neuronal damage in a mouse model of global cerebral ischemia. *Neurobiol. Stress* **5**, 8–18 (2016).
36. L. G. Koch, O. J. Kemi, N. Qi, S. X. Leng, P. Bijma, L. J. Gilligan, J. E. Wilkinson, H. Wisløff, M. A. Høydal, N. Rolim, P. M. Abadir, E. M. van Grevenhof, G. L. Smith, C. F. Burant, Ø. Ellingsen, S. L. Britton, U. Wisløff, Intrinsic aerobic capacity sets a divide for aging and longevity. *Circ. Res.* **109**, 1162–1172 (2011).
37. S. N. Rezvani, A. E. C. Nichols, R. W. Grange, L. A. Dahlgren, P. G. Brolinson, V. M. Wang, A novel murine muscle loading model to investigate Achilles musculotendinous adaptation. *J. Appl. Physiol.* **130**, 1043–1051 (2021).
38. L. H. Nakama, K. B. King, S. Abrahamsson, D. M. Rempel, Evidence of tendon microtears due to cyclical loading in an in vivo tendinopathy model. *J. Orthop. Res.* **23**, 1199–1205 (2005).
39. E. S. Boyden, A history of optogenetics: The development of tools for controlling brain circuits with light. *F1000 Biol. Rep.* **3**, 11 (2011).
40. G. Nagel, T. Szellas, W. Huhn, S. Kateriya, N. Adeishvili, P. Berthold, D. Ollig, P. Hegemann, E. Bamberg, Channelrhodopsin-2, a directly light-gated cation-selective membrane channel. *Proc. Natl. Acad. Sci. U.S.A.* **100**, 13940–13945 (2003).
41. K. Deisseroth, Optogenetics. *Nat. Methods* **8**, 26–29 (2011).
42. E. S. Boyden, F. Zhang, E. Bamberg, G. Nagel, K. Deisseroth, Millisecond-timescale, genetically targeted optical control of neural activity. *Nat. Neurosci.* **8**, 1263–1268 (2005).
43. P. Magown, B. Shettar, Y. Zhang, V. F. Rafuse, Direct optical activation of skeletal muscle fibres efficiently controls muscle contraction and attenuates denervation atrophy. *Nat. Commun.* **6**, 8506 (2015).
44. E. Ganji, C. S. Chan, C. W. Ward, M. L. Killian, Optogenetic activation of muscle contraction in vivo. *Connect. Tissue Res.* **62**, 15–23 (2021).
45. T. Bruegmann, T. van Bremen, C. C. Vogt, T. Send, B. K. Fleischmann, P. Sasse, Optogenetic control of contractile function in skeletal muscle. *Nat. Commun.* **6**, 7153 (2015).
46. J. L. Zitnay, Y. Li, Z. Qin, B. H. San, B. Depalle, S. P. Reese, M. J. Buehler, S. M. Yu, J. A. Weiss, Molecular level detection and localization of mechanical damage in collagen enabled by collagen hybridizing peptides. *Nat. Commun.* **8**, 14913 (2017).
47. Y. Li, C. A. Foss, D. D. Summerfield, J. J. Doyle, C. M. Torok, H. C. Dietz, M. G. Pomper, S. M. Yu, Targeting collagen strands by photo-triggered triple-helix hybridization. *Proc. Natl. Acad. Sci. U.S.A.* **109**, 14767–14772 (2012).
48. L. L. Bennink, Y. Li, B. Kim, I. J. Shin, B. H. San, M. Zangari, D. Yoon, S. M. Yu, Visualizing collagen proteolysis by peptide hybridization: From 3D cell culture to in vivo imaging. *Biomaterials* **183**, 67–76 (2018).

Downloaded from https://www.science.org on July 08, 2024

49. X. Lin, M. Huang, G. Yin, J. Zhang, Z. Zhang, P. Lai, B. Yan, Y. Chen, D. Jin, L. Wang, Characterization of a novel calcific achilles tendinopathy model in mice: Contralateral tendinopathy induced by unilateral tenotomy. *Calcif. Tissue Int.* **103**, 698–707 (2018).
50. N. S. Cho, J. H. Hwang, Y. T. Lee, S. W. Chae, Tendinosis-like histologic and molecular changes of the Achilles tendon to repetitive stress: A pilot study in rats. *Clin. Orthop. Relat. Res.* **469**, 3172–3180 (2011).
51. J. Pingel, J. Wienecke, M. Kongsgaard, H. Behzad, T. Abraham, H. Langberg, A. Scott, Increased mast cell numbers in a calcaneal tendon overuse model. *Scand. J. Med. Sci. Sports* **23**, e353–e360 (2013).
52. M. I. Almeida-Silveira, D. Lambertz, C. Pérot, F. Goubel, Changes in stiffness induced by hindlimb suspension in rat Achilles tendon. *Eur. J. Appl. Physiol.* **81**, 252–257 (2000).
53. Y. X. Liu, S. Thomopoulos, V. Birman, J.-S. Li, G. M. Genin, Bi-material attachment through a compliant interfacial system at the tendon-to-bone insertion site. *Mech. Mater.* **44**, 83–92 (2012).
54. G. M. Genin, A. Kent, V. Birman, B. Wopenka, J. D. Pasteris, P. J. Marquez, S. Thomopoulos, Functional grading of mineral and collagen in the attachment of tendon to bone. *Biophys. J.* **97**, 976–985 (2009).
55. J. Zhang, J. H.-C. Wang, Moderate exercise mitigates the detrimental effects of aging on tendon stem cells. *PLOS ONE* **10**, e0130454 (2015).
56. R. B. Svensson, K. M. Heinemeier, C. Couppé, M. Kjaer, S. P. Magnusson, Effect of aging and exercise on the tendon. *J. Appl. Physiol.* **121**, 1353–1362 (2016).
57. Y. Sugiyama, K. Naito, K. Goto, Y. Kojima, A. Furuhata, M. Igarashi, I. Nagaoka, K. Kaneko, Effect of aging on the tendon structure and tendon-associated gene expression in mouse foot flexor tendon. *Biomed. Rep.* **10**, 238–244 (2019).
58. M. Franchi, A. Trirè, M. Quaranta, E. Orsini, V. Ottani, Collagen structure of tendon relates to function. *Scientific World Journal* **7**, 404–420 (2007).
59. X. Wang; R. A. Bank, J. M. TeKoppele, C. M. Agrawal, The role of collagen in determining bone mechanical properties. *J. Orthop. Res.* **19**, 1021–1026 (2001).
60. P. Sharma, N. Maffulli, Tendon injury and tendinopathy: Healing and repair. *J. Bone Joint Surg. Am.* **87**, 187–202 (2005).
61. S. E. Szczesny, C. Aeppli, A. David, R. L. Mauck, Fatigue loading of tendon results in collagen kinking and denaturation but does not change local tissue mechanics. *J. Biomech.* **71**, 251–256 (2018).
62. M. Chatterjee, P. M. Muljadi, N. Andarawis-Puri, The role of the tendon ECM in mechanotransduction: Disruption and repair following overuse. *Connect. Tissue Res.* **63**, 28–42 (2022).
63. T. M. Ritty, R. Roth, J. E. Heuser, Tendon cell array isolation reveals a previously unknown fibrillin-2-containing macromolecular assembly. *Structure* **11**, 1179–1188 (2003).
64. S. P. Arnoczky, M. Lavagnino, M. Egerbacher, The mechanobiological aetiopathogenesis of tendinopathy: Is it the over-stimulation or the under-stimulation of tendon cells? *Int. J. Exp. Pathol.* **88**, 217–226 (2007).
65. H. B. Sun, N. Andarawis-Puri, Y. Li, D. T. Fung, J. Y. Lee, V. M. Wang, J. Basta-Pljakic, D. J. Leong, J. B. Sereysky, S. J. Ros, R. A. Klug, J. Braman, M. B. Schaffler, K. J. Jepsen, E. L. Flatow, Cycle-dependent matrix remodeling gene expression response in fatigue-loaded rat patellar tendons. *J. Orthop. Res.* **28**, 1380–1386 (2010).
66. J. B. Holt, J. M. Pedowitz, P. H. Stearns, T. P. Bastrom, M. M. Dennis, J. R. Dwek, A. T. Pennock, Progressive elbow magnetic resonance imaging abnormalities in little league baseball players are common: A 3-year longitudinal evaluation. *Am. J. Sports Med.* **48**, 466–472 (2020).
67. A. T. Pennock, J. Dwek, E. Levy, P. Stearns, J. Manning, M. M. Dennis, A. Davis-Juarez, T. Bastrom, K. S. Taylor, Shoulder MRI abnormalities in asymptomatic little league baseball players. *Orthop. J. Sports Med.* **6**, 2325967118756825 (2018).
68. A. G. Berman, J. M. Organ, M. R. Allen, J. M. Wallace, Muscle contraction induces osteogenic levels of cortical bone strain despite muscle weakness in a mouse model of Osteogenesis Imperfecta. *Bone* **132**, 115061 (2020).
69. H. Leblond, M. L'Espérance, D. Orsal, S. Rossignol, Treadmill locomotion in the intact and spinal mouse. *J. Neurosci.* **23**, 11411–11419 (2003).
70. K. G. Pearson, H. Acharya, K. Fouad, A new electrode configuration for recording electromyographic activity in behaving mice. *J. Neurosci. Methods* **148**, 36–42 (2005).
71. L. K. Ritter, M. C. Tresch, C. J. Heckman, M. Manuel, V. M. Tysseling, Characterization of motor units in behaving adult mice shows a wide primary range. *J. Neurophysiol.* **112**, 543–551 (2014).
72. S. V. Brooks, J. A. Faulkner, Contractile properties of skeletal muscles from young, adult and aged mice. *J. Physiol.* **404**, 71–82 (1988).
73. I. Kurtaliaj, M. Golman, A. C. Abraham, S. Thomopoulos, Biomechanical testing of murine tendons. *J. Vis. Exp.* 10.3791/60280, (2019).
74. M. I. Love, W. Huber, S. Anders, Moderated estimation of fold change and dispersion for RNA-seq data with DESeq2. *Genome Biol.* **15**, 550 (2014).
75. M. Stephens, False discovery rates: A new deal. *Biostatistics* **18**, 275–294 (2017).
76. S. Anders, W. Huber, Differential expression analysis for sequence count data. *Genome Biol.* **11**, R106 (2010).
77. D. W. Huang, B. T. Sherman, R. A. Lempicki, Systematic and integrative analysis of large gene lists using DAVID bioinformatics resources. *Nat. Protoc.* **4**, 44–57 (2009).
78. D. W. Huang, B. T. Sherman, R. A. Lempicki, Bioinformatics enrichment tools: Paths toward the comprehensive functional analysis of large gene lists. *Nucleic Acids Res.* **37**, 1–13 (2009).

Acknowledgments: We thank the Advanced Genomics Core at the University of Michigan for library preparation and next-generation sequencing. We also thank C. S. Davis and S. V. Brooks for the support provided for in vitro muscle contractility measurements and G. Caubel for preliminary imaging assistance using ShapeWorks. We thank E. Snyder-White and C. Whitinger for assistance with histology. Schematics were made using BioRender. **Funding:** This work was supported by funding from the National Science Foundation (CAREER #1944448). This work was also supported by funding from the National Institutes of Health (principal investigator (PI): M.L.K., "FGF signaling during growth and mechanical adaptation of tendon-bone interfaces," NIAMS-R01AR079367 and "Contributions of skeletal muscle loading during rotator cuff maturation and healing," NICHD-R03HD094594). Resources related to development of transgenic animal models was supported by NCI-P30CA046592 (PI: T. L. Saunders). Development and use of statistical shape modeling was supported by funding from the National Institutes of Health (PI: S. Y. Elhabian, "ShapeWorksStudio: An Integrative, User-Friendly, and Scalable Suite for Shape Representation and Analysis," NIBIB-U24EB029011; "Anatomy Directly from Imagery: General-purpose, Scalable, and Open-source Machine Learning Approaches," NIAMS-R01AR076120) and the Center for Integrative Biomedical Computing (PI: C. R. Johnson, NIGMS-P41GM103545). microCT was supported by funding from the National Institutes of Health (PI: T. S. Buchanan, "Osteoarthritis: Prevention and Treatment," NIGMS-P30GM103333; and PI: K. J. Jepsen, "The Michigan Integrative Musculoskeletal Health Core Center, NIAMS-P30AR069620). Library preparation and next-generation sequencing were carried out in the Advanced Genomics Core at the University of Michigan. Support for E.G. was from the Beckman Institute for Advanced Science and Technology, University of Illinois-Urbana-Champaign. Development of optogenetic mice was supported by funding from the Michigan-Israel Partnership for Research and Education. **Author contributions:** Conceptualization: E.G., S.N.L., M.S., N.W., A.C.A., and M.L.K.. Methodology: E.G., S.N.L., A.C.A., and M.L.K.. Investigation: E.G., S.N.L., and R.W.G. Visualization: E.G., S.N.L., R.W.G., and M.L.K.. Supervision: M.L.K.. Writing—original draft: E.G., S.N.L., M.S., N.W., A.C.A., and M.L.K.. Writing—review and editing: E.G., S.N.L., M.S., N.W., R.W.G., A.C.A., and M.L.K.. **Competing interests:** All authors declare that they have no competing interests. **Data and materials availability:** The RNA-seq data generated in this study are openly available in Gene Expression Omnibus (GEO) with a reference number GSE226742. All data needed to evaluate the conclusions in the paper are present in the paper and/or the Supplementary Materials.

Submitted 9 December 2022
Accepted 17 May 2023
Published 23 June 2023
10.1126/sciadv.adf4683

Downloaded from https://www.science.org on July 08, 2024